Title
The electrodynamic response of heavy-electron materials with magnetic phase transitions

Journal
Zeitschrift für Physik B Condensed Matter, 102(3)

ISSN
0722-3277

Authors
Degiorgi, L
Thieme, St
Ott, HR
et al.

Publication Date
1997-12-01

DOI
10.1007/s002570050300

Z. Phys. B 102, 367–380 (1997)

ZEITSCHRIFT
FÜR PHYSIK B

The electrodynamic response of heavy-electron materials with magnetic phase transitions

L. Degiorgi[1], St. Thieme[1], H.R. Ott[1], M. Dressel[2,*], G. Grüner[2], Y. Dalichaouch[3], M.B. Maple[3], Z. Fisk[4,], C. Geibel[5], F. Steglich[5]**

[1] Laboratorium für Festkörperphysik, ETH-Zurich, CH-8093 Zurich, Switzerland
[2] Department of Physics, University of California at Los Angeles, Los Angeles, CA 90095, USA
[3] Department of Physics, University of California at San Diego, La Jolla, CA 92093, USA
[4] Materials Science and Technology Division, Los Alamos National Laboratory, Los Alamos, NM 87545, USA
[5] Institut für Festkörperphysik, TH Darmstadt, D-64289 Darmstadt, Germany

Received: 3 July 1996/Revised version: 20 September 1996

Abstract. We have investigated the electrodynamic response of the heavy-electron compounds U_2Zn_{17}, UPd_2Al_3, UCu_5 and URu_2Si_2. Particular emphasis has been devoted to the optical evidence of the antiferromagnetic phase transitions at $T_N = 9.7$ K, 14 K, 15 K and 17 K for U_2Zn_{17}, UPd_2Al_3, UCu_5 and URu_2Si_2, respectively. In the excitation spectrum of UCu_5 and URu_2Si_2, we found an absorption in the far-infrared, which develops below T_N and is ascribed to the excitation across a spin-density-wave type gap, suggesting that the antiferromagnetic phase transition might be itinerant in nature, and invokes a Fermi surface instability. Since this gap-like feature is absent in U_2Zn_{17} and UPd_2Al_3, we argue that these latter compounds belong to a characteristically different class of antiferromagnets, representative of the heavy-electron compounds with an ordering of essentially localized magnetic moments. The antiferromagnetic ordering then leads to a suppression of the spin-flip mechanism below T_N. At low temperatures, we observe for all compounds the formation of a narrow Drude-like resonance in the optical conductivity, which is ascribed to the electrodynamic response of the heavy-quasiparticles, and is indicative of the progressive development of the many-body coherent Kondo state, coexisting with both types of magnetic ordering. In this review, we also present the evolution of the optical properties due to Ni- and Re-doping in UCu_5 and URu_2Si_2, respectively. The optical evidence of the itinerant antiferromagnetic ordering is suppressed in both compounds upon doping and particularly for the URu_2Si_2 compound this is consistent with a crossover to a ferromagnetic ground state upon Re-doping.

PACS: 78.20-e; 71.28 + d; 75.20.Hr

Introduction

The electrodynamic response of several heavy-electron (HE) metals, like $CeAl_3$, $CeCu_6$, $CePd_3$, UPt_3 etc., has been explored in detail [1–8]. The relevant physical quantity describing the electrodynamic response is the complex optical conductivity $\sigma(\omega)$, which displays a characteristic behaviour as soon as the HE systems cross the boundary between the incoherent (single Kondo) and many-body coherent (Kondo lattice) state. Such a crossover is defined by a characteristic temperature T_{CO} which usually coincides with a broad maximum found in the temperature dependence of the resistivity $\rho(T)$ of several HE materials. At $T \ll T_{CO}$, namely in the many body coherent state, the real part of the conductivity $\sigma_1(\omega)$ shows the formation of a narrow Drude-like resonance (i.e., centered at $\omega = 0$). Such a narrow resonance (see also Fig. 1 of Ref. 8) emerges progressively with decreasing temperature out of the high-temperature spectrum which generally follows a broader Drude behaviour above T_{CO} [1–8]. The narrow resonance is ascribed to the contribution of the heavy-quasiparticles to the optical conductivity. The small spectral weight of the resonance is related to the large effective mass m* of the heavy electrons via the sum rule argument

$$\int_0^{\omega_c} \sigma_1(\omega)\mathrm{d}\omega = \frac{\omega_p^{*2}}{8} = \frac{\pi n e^2}{2m^*}, \tag{1}$$

where n is the charge carrier concentration and ω_C is a cut-off frequency, defined by the roll off of the narrow Drude component in $\sigma_1(\omega)$ [1–8]. The narrow Drude-like resonance may be related with a small scattering rate $1/\tau^*$, as well. The experimental $\sigma_1(\omega)$ follows very closely the theoretical prediction, for which the enhancement of the scattering relaxation time below T_{CO} should go hand in hand with the corresponding enhancement of the effective mass (i.e., $\tau^*/\tau = m^*/m_b$, where m_b is the mass and τ is the unrenormalized scattering time) [9, 10].

Significantly less is known about the electrodynamics of the superconducting and magnetic states of these materials. Although magnetic ordering and heavy-electron

* *Present address*: Institut für Festkörperphysik, TH Darmstadt, D-64289 Darmstadt, Germany
** *Present address*: Department of Physics and National High Magnetic Field Laboratory, Florida State University, Tallahassee, FL 32306, USA

behaviour, eventually together with superconductivity, seem, at first sight, to be mutually exclusive, various experimental observations in recent years indicate that this is not necessarily the case. Both magnetic ordering out of a heavy-electron state and the formation of a heavy-electron state in a magnetically-ordered matrix seem possible. Examples of these two distinctly different situations are realized in the low-temperature properties of U_2Zn_{17} [11] and UCu_5 [12], which order antiferromagnetically at 9.7 K and 15 K, respectively.

Superconductivity in HE materials, like, e.g., $CeCu_2Si_2$, UPt_3 and UBe_{13} is also a fascinating topic [13, 14]. Of particular interest are those HE materials showing the coexistence of superconductivity with magnetic ordering. In this respect, URu_2Si_2 attracted a lot of attention as the first HE metal with superconductivity ($T_c = 1$ K), developing in an antiferromagnetically ordered matrix ($T_N = 17.5$ K) [15]. More recently, a systematic search led to the discovery of the coexistence of antiferromagnetism and superconductivity in UNi_2Al_3 ($T_N = 4.6$ K and $T_c = 1$ K) and UPd_2Al_3 ($T_N = 14$ K and $T_c = 2$K) [16, 17], as well.

In this review, we will focus our attention on the antiferromagnetic (AFM) phase transitions, which are indicated by distinct anomalies of the specific heat and abrupt changes in the temperature dependence of the magnetic susceptibility. Neutron-diffraction experiments for U_2Zn_{17}, UCu_5, URu_2Si_2 and UPd_2Al_3 [18–21] reveal rather conventional types of arrangements of the ordered moments which are of about 1 μ_B for U_2Zn_{17}, UCu_5 or UPd_2Al_3, and 0.01 μ_B for URu_2Si_2 [18–21]. However, μSR measurements on U_2Zn_{17} have indicated that the magnetic properties are not as simple as implied by neutron diffraction results [22]. In fact, a non uniform magnetic behaviour was found and only a small fraction of the U-5f moments is compatible with the simple antiferromagnetic order suggested by neutron diffraction studies.

The ordering temperatures (T_N) can also be precisely identified by non-monotonic variations of the temperature dependence of the electrical resistivity (Fig. 1). For U_2Zn_{17} and UPd_2Al_3, the positive slope $\delta_\rho/\delta T$ suddenly increases with decreasing temperature, manifesting lesser scattering of conduction electrons at moment fluctuations (Fig. 1a and 1b) [11]. For UCu_5 and URu_2Si_2 the behaviour of $\rho(T)$ is distinctly different (Fig. 1c and 1d) [12, 23, 24]. The dc resistivity increases at the antiferromagnetic transition, indicating the partial removal of the Fermi surface. Decaying magnetic scattering and the onset of coherence, as the heavy-electron state develops well below T_N, result in a maximum of $\rho(T)$ approximately 3 K below the Neel temperature [12, 23, 24]. Consequently, the $\rho(T)$ variation close to but below T_N in the latter two compounds implies that the energy spectrum of the itinerant charge carriers is considerably affected by the phase transition, in contrast to the observation in U_2Zn_{17} [11] and UPd_2Al_3 [16]. For both UCu_5 and URu_2Si_2, the magnetic state is supposed to develop as the consequence of a Fermi surface anomaly, similar to the one at the spin-density-wave (SDW) transition in Cr [25]. Such a SDW instability is representative of an itinerant-like AFM ordering. On the other hand, for U_2Zn_{17} and UPd_2Al_3 the AFM should be the consequence of a freezing of the spin flip scattering mechanism, which implies a magnetic phase transition of localized type [11].

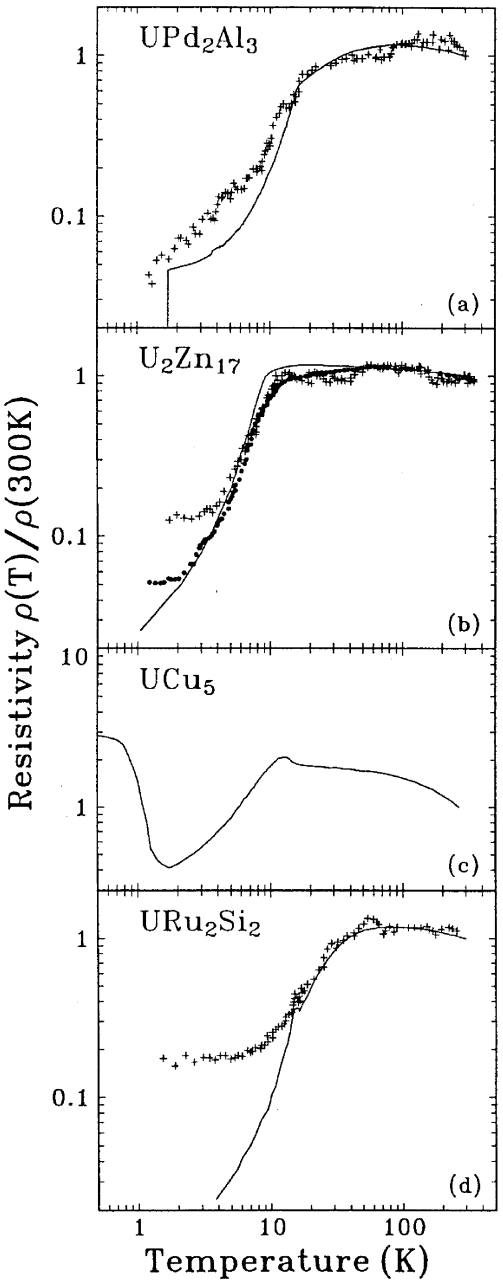

Fig. 1. Temperature dependence of the electrical resistivity (continuous line) of **a** UPd_2Al_3, **b** U_2Zn_{17}, **c** UCu_5, and **d** URu_2Si_2, normalized to the resistivity values at 300 K. (●) and (+) refer to the 35 and 100 GHz measurements, respectively

The AFM phase transitions discussed here are very sensitive to the chemical composition of these materials. For instance, the antiferromagnetic ordering is suppressed by replacing Cu and Zn by small amount (1–2%) of Ni and Cu in UCu_5 and U_2Zn_{17}, respectively [26]. It has also been established that a ferromagnetic ground state develops in URu_2Si_2 by replacing Ru with Re and Tc [27]. Therefore, the materials $URu_{2-x}Re_xSi_2$ present the unique possibility to scan a rather complex magnetic phase diagram, which extends from an itinerant

antiferromagnetic or SDW-like ground state, with a rather small ordered U-moment for $x < 0.2$, to a ferromagnetic state with maximum magnetic moments of $0.44 m_B$/Uatom for $0.4 < x < 1.4$ [27]. The large value of the specific heat γ-value also suggests that both antiferromagnetism and ferromagnetism are associated with a narrow feature in the density of states of a band of strongly correlated electrons [27].

Here, we report on our attempts to study these features in more depth by probing the effects of the magnetic phase transitions with optical methods. The optical experiments are very suitable because an *incommensurate* antiferromagnetic order (i.e, itinerant) should lead to a spin-density-wave formation and an opening of a gap at the Fermi level ε_F, causing a distinct absorption in the excitation spectrum at $2\Delta = 3.52\, k_B T_N$. Such a SDW arises as a result of the Fermi-surface instability, due to the degeneracy between occupied levels on one side and empty levels on the other side of the Fermi-distribution edge. First optical experiments on URu_2Si_2 gave evidence for a single particle gap [28] in analogy to the optical results of Cr [25]. In the case of a *commensurate* antiferromagnetic order (i.e., localized moments) we would not expect a gap at ε_F for partially filled bands. In fact, large band structure gaps are due to the periodic crystal potential and new gaps at ε_F would open only in the unlikely situation where the lattice potential is very weak [29]. Therefore, we should be able to discriminate between these two scenarios (i.e., itinerant or localized) depending whether the magnetic ordering leads to a gap formation or not. We also applied our optical spectroscopy methods in order to follow the effect of doping on the magnetic phase transition and particularly the optical evolution from a $q = 2k_F$ anomaly (SDW) towards a $q = 0$ ferromagnetic phase in $URu_{2-x}Re_xSi_2$.

The paper is organized as follows: a description of the samples' preparation and of the various experimental techniques will be followed by a full review of the experimental results. Subsequently, we discuss the data comparing the contrasting electrodynamic response found in either UPd_2Al_3 and U_2Zn_{17}, or in UCu_5 and URu_2Si_2, respectively. The concluding paragraph will summarize the major and most relevant achievements, establishing a comparison with the broad class of the typical HE systems (like, e.g., UPt_3). Some of the results have been already presented elsewhere [30–32].

Experiment and results

a) *Sample preparation and characterization*

The single crystals of URu_2Si_2 and UPd_2Al_3 used for this optical work have been grown in a tri-arc furnace, using the Czochralski technique. The polycrystalline specimens of $URu_{2-x}Re_xSi_2$, UPd_2Al_3, $UCu_{5-x}Ni_x$ and U_2Zn_{17}, on the other hand, were prepared by arc melting the appropriate amounts of high-purity elements in an argon atmosphere [11, 12, 16, 27]. All samples were then vacuum annealed for a few days at high temperatures of about 900°C, in order to remove remaining secondary phases and to improve the lattice perfection. The optical results of UPd_2Al_3 and URu_2Si_2 are identical for both single or polycrystalline specimens. Here, we will report on our latest results on well crystallographically oriented single crystals. As far as U_2Zn_{17} and UCu_5 are concerned, only well-annealed polycrystalline samples have been used for our optical investigations. However, previous experiments [11] on U_2Zn_{17} have shown that all features of the low-temperature properties are independent of whether they are measured on poly-or single-crystalline material. Moreover, we note that for UCu_5 we have investigated the same specimen, previously used for studies of low-temperature transport properties [23]. For the other compounds, we choose specimens from the same batches already used for transport and thermodynamic investigations.

A variety of experiments has been employed in order to characterize the specimens, like, e.g., X-ray diffraction, magnetization and resistivity measurements. The temperature dependence of the resistivity $\rho(T)$ (see Fig. 1) clearly shows the main features described above in the introduction. The non-monotonic behaviour of $\rho(T)$ at the phase transition, in form of an anomaly, where $\rho(T)$ reaches a maximum a few Kelvin below the transition temperature, or with a sudden change in slope, defines the Neel temperature T_N or the Curie temperature T_C for the antiferromagnetic and ferromagnetic phase transitions, respectively. URu_2Si_2 and UPd_2Al_3 display, moreover, the sharp drop to the superconducting ground state of T_c.

b) *Experimental techniques*

The reflectivity $R(\omega)$ has been measured on a broad frequency spectral range between $15\ cm^{-1}$ and $10^5\ cm^{-1}$, using four spectrometers with overlapping frequency intervals. In the far-infrared (FIR) we made use of a Bruker IFS113v Fourier interferometer, while from the FIR up to the mid-IR we used a fast scanning Bruker interferometer IFS48PC. In the visible and ultra-violet (UV) spectral range we employed a home-made spectrometer based on a Zeiss monochromator and a McPherson spectrometer, respectively. From the mid-IR down to the FIR we have used the reflectivity of gold as reference [8]. The crystals had polished surfaces. We have observed that the polishing procedure only increases the overall reflectivity without any other qualitative changes relative to the measurements previously performed on the unpublished surfaces.

At millimeter and microwave frequencies the optical properties were obtained with cavity perturbation techniques [33]. We measured the optical conductivity at 35 and 100 GHz by placing the sample or a small piece of it in the maximum of the electric field of a cylinderical TE_{011} microwave cavity. From the change of the quality factor, the conductivity was evaluated using standard cavity perturbation theory [33], assuming the Hegen-Rubens (HR) relation between the surface resistance R_s and the conductivity σ_1:

$$\sigma_1 = \frac{2\pi\omega}{c^2 R_s^2} \tag{2}$$

From the surface resistance R_s we can also evaluate the corresponding absorptivity:

$$A(\omega) = \frac{4R_s}{Z_0} \tag{3}$$

where $Z_0 = 377\,\Omega$ is the impedance of the free space. Equation (3) holds if R_s and $|X_s| \ll Z_0$, which is always the case for metallic samples. $A(\omega) = 1 - R(\omega)$ can be combined with the reflectivity measurements obtained on a continuum of frequencies from the FIR up to the UV. Consequently, the total optical conductivity $\sigma_1(\omega)$ is obtained through Kramers-Kronig (KK) transformations of the $R(\omega)$ spectra, extending over several decades in frequency. At higher frequencies, we applied the usual extrapolations $R(\omega) \sim 1/\omega^2$ for $\omega < 3 \times 10^5\,cm^{-1}$ and $R(\omega) \sim 1/\omega^4$ above. The extrapolation, below the lowest measurable frequency towards zero, was performed with the help of the Hagen-Rubens relation:

$$R(\omega) = 1 - 2\sqrt{\frac{\omega}{2\pi\sigma_{dc}}} \tag{4}$$

where the static conductivity σ_{dc} is obtained from the dc transport data [11, 12, 15–17, 27].

c) Results

UPd_2Al_3. Figure 1a displays the temperature dependence of the normalized resistivity of UPd_2Al_3 at dc and 100 GHz. The latter measurement is very similar to the dc behaviour, thus suggesting that below the FIR spectral range the system enters in the so-called HR regime. The dc resistivity $\rho_{dc}(T)$ exhibits a maximum at about 80 K, marked as the temperature T_{CO}, a shoulder at T_N and the sharp drop to zero at T_c. Besides the two phase transitions at T_N and T_c, the overall behaviour of $\rho(T)$ bears a close similarity with the transport properties of other HE's [13, 14, 26]. Above $T_{CO} = 80$ K (i.e., in the incoherent regime), $\rho(T)$ decreases with increasing temperature in a manner similar to that observed in metals containing isolated magnetic impurities, thus suggesting a single-ion Kondo scattering mechanism. Below T_{CO} (i.e., in the coherent regime) where the many body effects progressively develop, $\rho(T)$ decreases with decreasing temperature until at the AFM transition at $T_N = 14$ K, where $\rho(T)$ reflects the freezing out of spin-disorder scattering.

Figure 2a displays $R(\omega)$ of UPd_2Al_3 parallel to the ab-plane of the hexagonal structure at several chosen temperatures above and below T_{CO} and T_N. Measurements along the c-axis and early investigations on polycrystalline samples gave similar result [30, 34]. The inset of Fig. 2a shows the FIR frequency range in detail for the ab-plane. $R(\omega)$ at temperatures close to and below T_{CO} is generally lower than $R(\omega)$ at 300 K. Around 100 cm^{-1} the reflectivity at 20 K merges with that at 300 K, while there is a crossover to higher reflectivity at 6 K and 15 K. This is a quite general behaviour of the optical properties of HE's (see below). UPd_2Al_3 does not show any significant changes in $R(\omega)$ when the temperature decreases below T_N.

The optical conductivity $\sigma_1(\omega)$, obtained through KK transformation of $R(\omega)$, is shown in Fig. 2b. Our $R(\omega)$

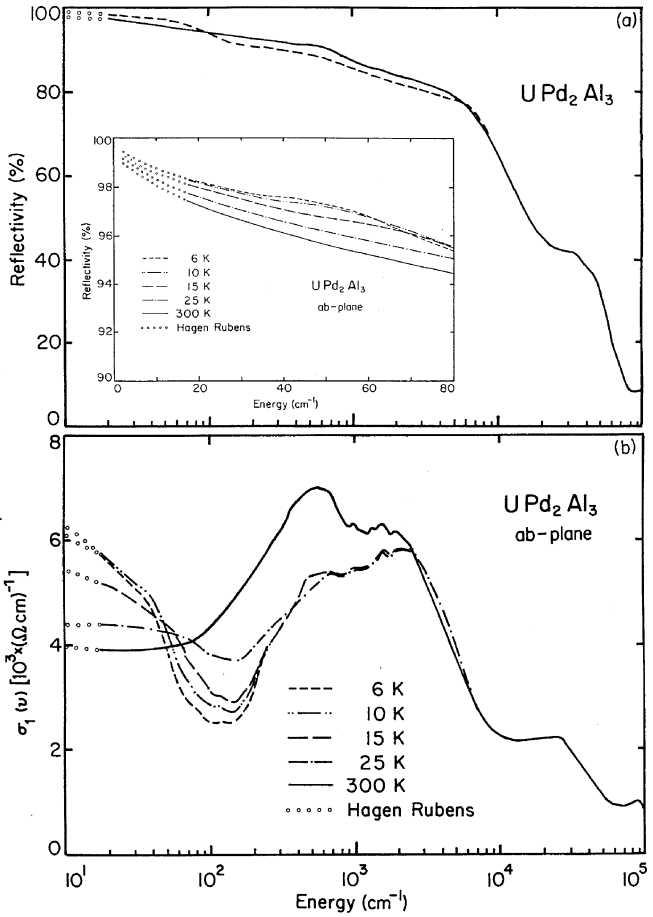

Fig. 2. a Reflectivity and **b** optical conductivity of UPd_2Al_3 at several temperatures in the whole investigated frequency range (note the logarithmic scale) in the ab-plane. The inset displays the FIR part (linear scale) of the reflectivity on an expanded scale

spectra in the FIR together with the microwave point at 100 GHz are consistent with a HR extrapolation making use of σ_{dc} values somewhat lower than the published ones [17, 35]. This can be also seen in the dc-limit (i.e. $\sigma_1(\omega \to 0)$) of our optical conductivity. Nevertheless, the relative temperature dependence of σ_{dc} is consistent with the $\omega \to 0$ limit of our FIR optical conductivity. We also notice the quite remarkable removal of spectral weight (i.e., eq. (1) in the limit of $\omega_c \to \infty$) between approximately 100 and 2000 cm^{-1} by decreasing the temperature from 300 K to 6 K. The removed spectral weight shifts to higher frequencies in the mid-IR spectral range, so that the total spectral weight is conserved (within the experimental error). At low temperatures in accordance with the FIR behaviour of $R(\omega)$, we observe the formation of a temperature dependent narrow Drude-like resonance. Similarly to $R(\omega)$, the temperature dependence of $\sigma_1(\omega)$ in FIR is not correlated with the onset of AFM at T_N.

U_2Zn_{17}. The temperature dependence of the dc resistivity of U_2Zn_{17} together with the results obtained at 35 and 100 GHz is presented in Fig. 1b. The microwave measurements follow the dc behaviour over a very large temperature regime above and below T_N. However, below

approximately 5 K, we recognize a frequency dependence of the resistivity, contrary to the situation encountered for UPd_2Al_3.

In Fig. 3a we present the room temperature reflectivity spectra in our accessible frequency range. The inset displays the R(ω) spectra at temperatures above and below T_N in the FIR range. At frequencies above the mid-IR there is no temperature dependence discernible in the reflectivity spectra. Figure 3b displays the excitation from FIR up to UV in terms of the optical conductivity for $T = 300$ K and for $T < T_N$. The excitation spectra in the mid-IR frequency range are dominated by an absorption, centered at 4000 cm^{-1}. In the ultraviolet some weak structures, probably due to electronic interband transitions, may be identified. The $\omega \to 0$ limit below the FIR spectral range of R(ω) and, above all, of $\sigma_1(\omega)$ at low temperatures would be consistent with an HR extrapolation with a σ_{dc} value lower than that at room temperature. This contradicts, however, the ρ(T) result (Fig. 1b), since $\sigma_1(\omega \to 0, 6\,K) \sim 300\ (\Omega cm)^{-1}$, while $\sigma_{dc}(6\,K) \sim 23000\ (\Omega cm)^{-1}$. This contradictory behaviour demonstrate the importance of performing optical investigations at low frequencies and temperatures. In fact, the apparent disagreement between the dc-limit of our optical properties inferred from the FIR spectral range and the dc transport data at low temperatures (i.e., 6 K) can be reconciled by considering the microwave results. From the measurements of the surface resistance R_s at 35 and 100 GHz (Fig. 1b), one can calculate σ_1 using (2). Even though the HR assumption implicit in (2) might be too crude [8, 36–38], it is gratifying that at low temperatures we obtain a fairly strong frequency dependence of $\sigma_1(\omega)$ by combining the FIR spectra with the microwave data. Such a frequency dependence of σ_1 will later be associated with the development of a narrow Drude-like resonance emerging at frequencies below the FIR spectral range. This narrow Drude-like behaviour re-establishes a fair agreement between the transport results and the optical properties so that now $\sigma_1(\omega \to 0, 6\,K) \sim \sigma_{dc}(6\,K)$.

UCu_5 and UNi_xCu_{5-x}. Figure 1c displays the temperature dependence of the resistivity of UCu_5 [12, 23], characterized by the two well known anomalies due to the AFM transition at T_N and to the yet unsettled transition below 1 K. The anomaly at T_N in ρ(T) overlaps with the broad resistivity maximum, usually defining T_{CO}. In other words, the AFM transition is close to a crossover from a single ion incoherent to a many body coherent Kondo regime.

The optical reflectivity of UCu_5 is shown in Fig. 4a and the corresponding optical conductivity in Fig. 4b. An

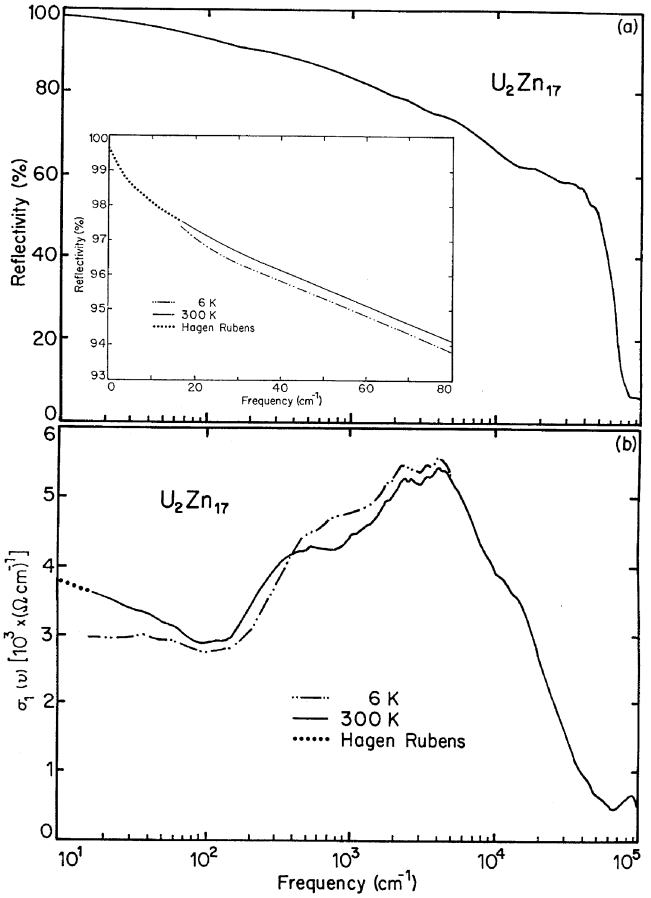

Fig. 3. **a** Reflectivity and **b** optical conductivity of U_2Zn_{17} at 6 and 300 K in the whole investigated frequency range (note the logarithmic scale). The inset displays the FIR part (linear scale) of the reflectivity on an expanded scale

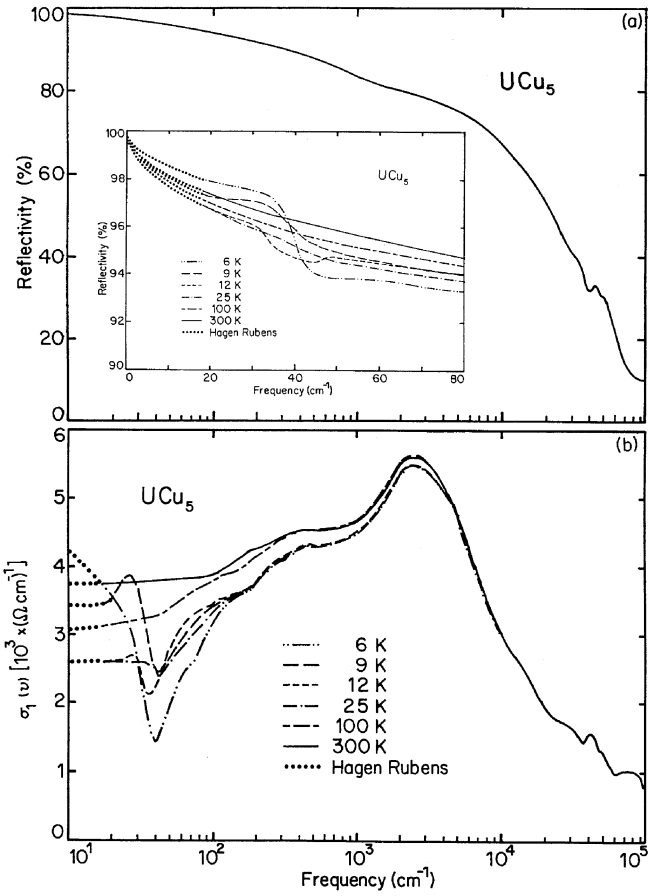

Fig. 4. **a** Reflectivity and **b** optical conductivity of UCu_5 at several temperatures in the whole investigated frequency range (note the logarithmic scale). The inset displays the FIR part (linear scale) of the reflectivity on an expanded scale

enlargement of R(ω) in the FIR spectral range is displayed in the inset of Fig. 4a. Contrary to the previous two cases, there is a remarkable temperature dependence of the optical properties below the antiferromagnetic phase transition at T_N. At 25 K the reflectivity has the typical metallic behaviour, while at 12 K, where a maximum of ρ(T) is observed [12, 23] we note a deviation from the usual metallic Drude-like behaviour in R(ω) at about 40 cm^{-1}. As shown in the inset of Fig. 4a, the magnitude of this anomaly grows with decreasing temperature. The lowest frequency part of R(ω) (Fig. 4a) at each temperature matches very well a HR extrapolation to 100% reflectivity at $\omega = 0$, taking into account the previously measured $\sigma_{dc}(T)$ values [23].

In the frequency range around 30 cm^{-1} the temperature dependence of R(ω) produces a very weak bump at 12 K, a well defined absorption at 9 K and a damped shoulder at 6 K in $\sigma_1(\omega)$ (Fig. 4b). We consider it important to note, that the general behaviour of $\sigma_1(\omega)$ in the measured frequency range (i.e., in FIR) is completely unaffected by the HR extrapolation. In fact, the evaluation of this part of the spectrum is fairly delicate and $\sigma_1(\omega)$ might the altered by ways of different extrapolations. We checked this aspect, by performing the KK transformations with an extension of the spectra other than the HR extrapolation. The bump or absorption at about 30 cm^{-1} in $\sigma_1(\omega)$ turns out to be even more enhanced in that case. Thus, we consider the performed extrapolation as a safe approach for the analysis of the optical spectra.

Figure 5 presents the R(ω) and $\sigma_1(\omega)$ spectra of the Ni-doped UCu_5 at 300 and 10 K. We found a temperature dependence of $\sigma_1(\omega)$ in FIR which is very reminiscent of the behaviour encountered in UPd_2Al_3 (Fig. 2). The temperature dependence of the conductivity $\sigma_1(\omega)$ displays the formation of a narrow Drude-like resonance at low temperatures and frequencies. However, we did not find any temperature dependence below 30 K and, contrary to the undopped UCu_5, the FIR feature at about 40 cm^{-1} is completely suppressed. This is in accordance with the transport and specific heat measurements where the anomalies associated with the AFM phase transition in UCu_5 vanish upon replacing even a small fraction of Cu with Ni [26].

URu_2Si_2 and $URu_{2-x}Re_xSi_2$. Figure 1d shows ρ(T) of URu_2Si_2 at dc and at 100 GHz, with an anomaly at T_N and a frequency dependence of the resistivity well below T_N. Contrary to UCu_5, the anomaly at T_N in URu_2Si_2 develops well below the broad maximum of ρ(T) at T_{CO}; namely,in the coherent Kondo regime where heavy charge carriers have already been formed.

Figure 6a and 6b, and the inset of Fig. 6a display the reflectivity and the optical conductivity in the whole measured frequency range and in FIR, respectively. In both R(ω) and $\sigma_1(\omega)$ there is a good agreement with the HR extrapolation, making use of the dc-conductivity data [15, 24]. The temperature dependence of R(ω) and $\sigma_1(\omega)$ is even more astonishing and remarkable than in UCu_5. Indeed, there is a well defined absorption, which appears at 60 cm^{-1} in coincidence with the onset of the antiferromagnetic phase transition at T_N. Our results are very similar to a previous report in the FIR-MIR spectral range by Bonn et al. [28]. Below the absorption at about 60 cm^{-1}, we recognize the FIR tail of the narrow Drude-like resonance, which is associated to the metallic contribution to $\sigma_1(\omega)$ due to the heavy quasiparticles. The absorption at 60 cm^{-1} in URu_2Si_2 bears a striking similarity with the absorption at 40 cm^{-1} in UCu_5. This FIR absorption appears more clearly in URu_2Si_2 than in UCu_5 because it is well separated from the contribution of the (remaining) heavy itinerant charge carriers (see below).

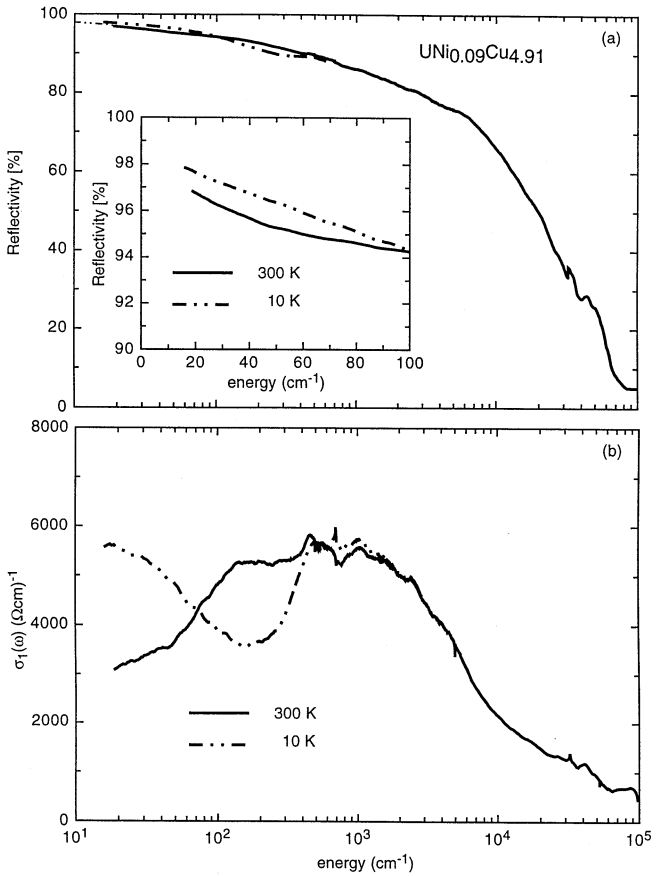

Fig. 5. **a** Reflectivity and **b** optical conductivity of $UNi_{0.09}Cu_{4.91}$ at several temperatures in the whole investigated frequency range (note the logarithmic scale). The inset displays the FIR part (linear scale) of the reflectivity on an expanded scale

Figure 7 compares the optical reflectivity and conductivity measured at 6 K for different Re-doping. Also for these doped systems, there is a satisfactory agreement between the low-frequency HR extrapolation and the transport data [27]. It is obvious that the absorption at about 60 cm^{-1} changes with the Re-doping content. In fact, as shown in Fig. 7b, this feature first shifts to lower frequency with increasing doping (i.e., $x = 0.05$ and $x = 0.1$) and then disappears for high Re-doping (i.e., $x > 0.4$). Therefore, upon entering the ferromagnetic state [27] in $URu_{2-x}Re_xSi_2$ not only the anomaly at T_N in ρ(T) but also the FIR absorption is progressively suppressed.

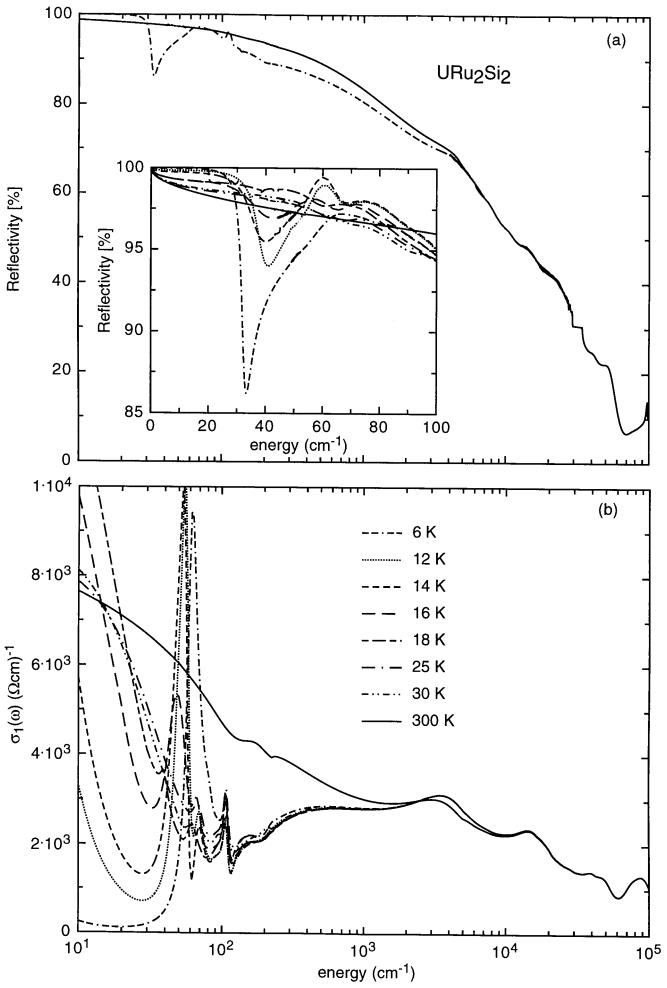

Fig. 6. a Reflectivity and **b** optical conductivity of URu_2Si_2 at several temperatures in the whole investigated frequency range (note the logarithmic scale). The inset displays the FIR part (linear scale) of the reflectivity on an expanded scale

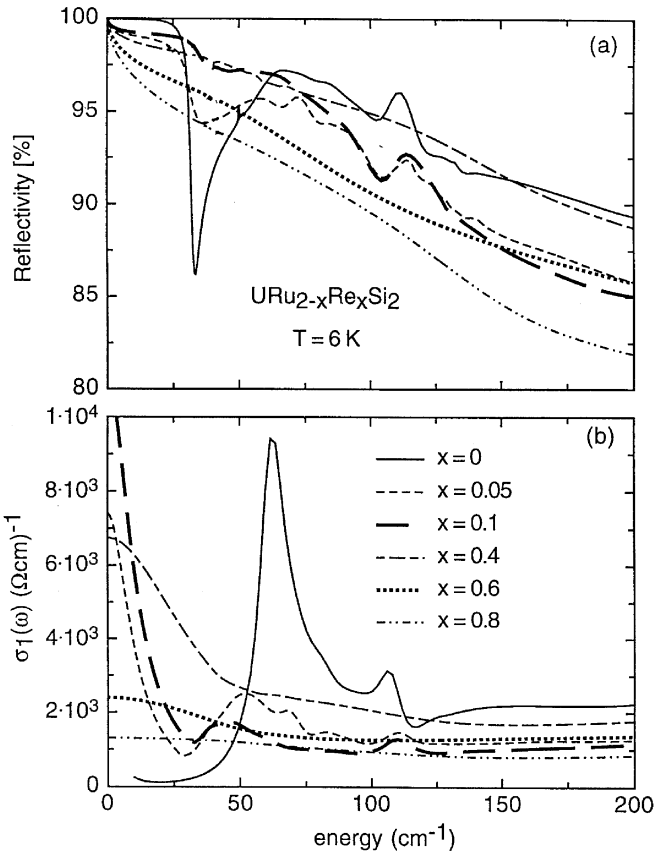

Fig. 7. Far-infrared reflectivity and optical conductivity of $URu_{2-x}Re_xSi_2$ for different Re-doping at 6 K

Discussion

The above presentation of the experimental data gives evidence of two classes of behaviour. For UCu_5 and URu_2Si_2 there are remarkable changes in the optical spectra at temperature below the AFM phase transition. A new absorption in FIR clearly develops below T_N. On the other hand, U_2Zn_{17} and UPd_2Al_3 are, from this point of view, quite different since their spectra seem to be unaffected by the development of the AFM order. No new absorption or deviation from a more or less conventional metallic behaviour have been detected in the vicinity of T_N. Similarly, the Ni-doped UCu_5 and the Re-doped URu_2Si_2 display a suppression of the FIR feature found at the onset of the AFM transition in the original binary and ternary compounds. In the following discussion, we will treat these two classes separately.

In the interpretation and discussion of the experimental data, we will rely on a simple phenomenological approach, based on the classical dispersion theory [39]. The optical conductivity can generally be approximated by a sum of Lorentz harmonic oscillators (h.o.) and of the Drude term. The former contributions arise each time an absorption at finite frequency takes place and they are usually ascribed to vibrational IR active modes (phonons) or/and to electronic interband transitions. The precise nature and origin of the considered h.o. will be specified later in the discussion of the different compounds. The Drude term applies for metals and describes the free charge carriers contribution to the electrodynamic response. The general formula for the complex dielectric function is:

$$\tilde{\varepsilon}(\omega) = \varepsilon_\infty - \frac{\omega_p^2}{\omega(\omega + i\Gamma)} + \sum_j \frac{\omega_{p,j}^2}{(\omega_j^2 - \omega^2) - i\Gamma_j\omega} \qquad (5)$$

where ω_p and $\Gamma \sim 1/\tau$ in the Drude term are the plasma frequency and the damping (i.e., scattering relaxation rate) of the free charge carriers, while ω_j, Γ_j and ω_{pj} are the resonance frequency, the damping and the mode strength of the harmonic oscillators, respectively. The high frequency absorptions above the UV spectral range are taken into account by ε_∞. This phenomenological fit is a useful approach in order to decouple the various components determining the excitation spectrum and to evaluate several intrinsic parameters (like, e.g., the plasma frequency and the scattering relaxation rate) which can be afterwards compared with similar quantities arrived at by other experiments.

The discussion is thus divided into two parts; the electrodynamic response of U_2Zn_{17} and UPd_2Al_3 will be analysed first and afterwards that of UCu_5 and URu_2Si_2, and of their Ni- and Re-doped alloys.

a) U_2Zn_{17} and UPd_2Al_3

For these two compounds we find no appreciable variation in the temperature dependence of $R(\omega)$ in FIR when decreasing the temperature below the corresponding AFM phase-transition temperature. Down to the FIR frequency range there is no indication of any new absorption appearing below T_N in $\sigma_1(\omega)$ (Figs 2 and 3). This is also clearly seen in Figs. 8 and 9 where blow-ups of the low-frequency parts of the excitation spectra are shown.

The temperature dependence in $\sigma_1(\omega)$ is due to a temperature dependent narrow Drude-like resonance in the FIR range for UPd_2Al_3 (Fig. 8) or in the GHz frequency spectral range for U_2Zn_{17} (Fig. 9). This latter behaviour in the optical conductivity is ascribed to the heavy-quasiparticles. In fact, the low frequency narrow Drude resonance is reminiscent of what has previously been found in prototype heavy-electron materials like, e.g., $CeAl_3$ [8] and UPt_3 [2, 3, 7], and corresponds to the expected manifestation of heavy quasiparticles in the electrodynamic response [9, 10].

In the spirit of (5), one can rewrite the Drude term with the plasma frequency $\omega_p^* = \omega_p/\sqrt{m^*/m_b}$ and the scattering relaxation time $\tau^* = \tau m^*/m_b$, which correspond to the bare quantities ω_p and τ being renormalized by the enhanced effective mass m^* of the heavy quasiparticles at low temperatures. A finite number of harmonic oscillators must be added in order to take into account the high frequency absorptions (see (5)). We associate the high frequency absorptions with electronic interband transitions and band structure effects. For UPd_2Al_3, there seems to be a satisfactory agreement with the electronic transitions inferred from the band structure calculations [40]. However, the calculation of the joint density of states from the electronic band structure would allow a more direct comparison, particularly with respect to the resonance frequency and excitation strength. The relevant fit parameters (i.e., for the Drude term) are listed in Table 1, for both U_2Zn_{17} and UPd_2Al_3. Figure 9 displays the fit for U_2Zn_{17} at 6 K in the microwave-FIR spectral range, and also the low temperature renormalized Drude component due to the electrodynamic response of the heavy quasiparticles [9, 10].

For UPd_2Al_3, the renormalized plasma frequency ω_p^* can be also calculated from the Pippard formula for the penetration depth,

$$\lambda = \frac{c}{\omega_p^*}\sqrt{1+\frac{\xi}{\ell}} \tag{6}$$

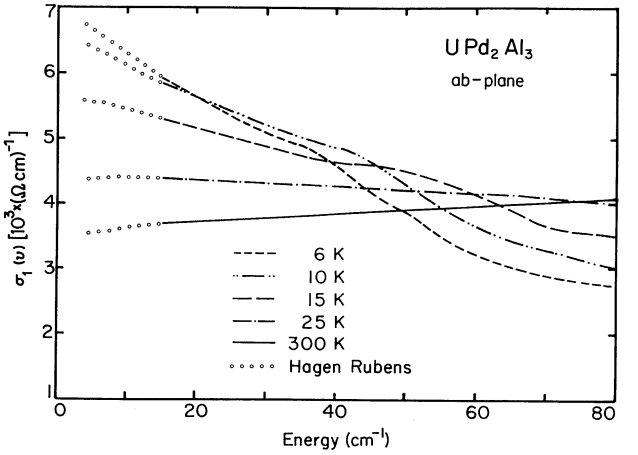

Fig. 8. Optical conductivity at several temperatures in the FIR energy range (linear energy scale) for UPd_2Al_3

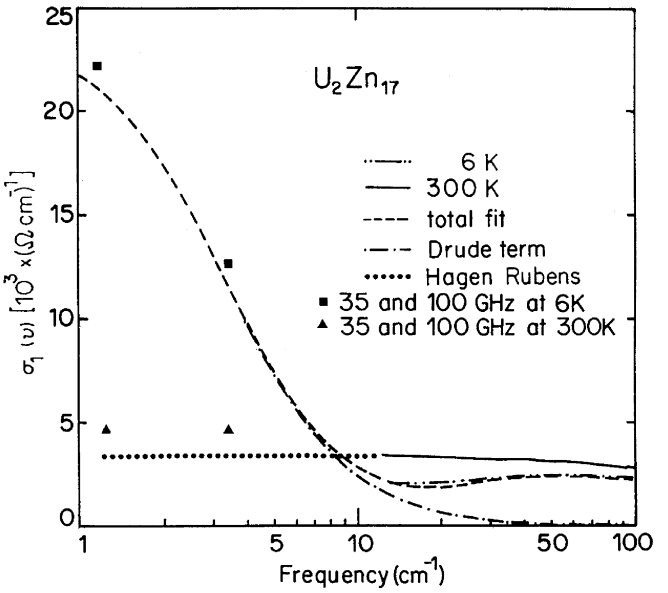

Fig. 9. Optical conductivity of U_2Zn_{17} in the FIR frequency range at 300 and 6 K together with the measurements at 35 and 100 GHz. The fit at 6 K and its renormalized Drude component are also shown (see text and Table 1 for the fit parameters)

Table 1. Relevant fit parameters of the Drude-Lorentz phenomenological approach of (5). The table displays the plasma frequency and the scattering relaxation rate at 300 K (ω_p and Γ) and at low temperature in the many body coherent state (ω_p^* and Γ^*). All values are in cm^{-1}. Moreover, the low temperature SDW-gap (2Δ, in cm^{-1}) and m^*/m_b calculated after (7) are also given

	ω_p	Γ	ω_p^*	Γ^*	$2\Delta(T = 6K)$	m^*/m_b
UPd_2Al_3	4.4×10^4	8545	4775	60	–	85
U_2Zn_{17}	1.4×10^4	1000	2178	3.33	–	41
UCu_5	2.83×10^4	3593	2600	22	28	95
URu_2Si_2	2.1×10^4	4853	2131	13	63	68

which takes into account the mean free path correction in the superconducting state. Here ℓ and ξ are the mean free path and the coherence length, respectively. Using the values $\lambda = 4000$–6500 Å and $\ell/\xi \sim 10$ quoted in [17] and [41] we obtain $\omega_p^* = 2568$–$4173\ cm^{-1}$ (0.32–0.52 eV), which is in fair agreement with our estimate from the renormalized Drude fit of $\sigma_1(\omega)$.

More generally, we can also compare our value of the renormalized plasma frequency ω_p^* at low temperatures (i.e., well within the AFM regime) with the Sommerfeld coefficient $\gamma(T \to 0)$ obtained from the electronic contribution of the specific heat of the normal state, in order to calculate the enhancement of the effective mass m* and the total charge carrier concentration n. From $\omega_p^* \propto (n/m^*)^{1/2}$ and $\gamma \propto m^* n^{1/3}$, we obtain for UPd_2Al_3 $m^* = 100 m_b$ and $n_e = 2.6 \times 10^{22}\ cm^{-3}$ using $\omega_p^* = 4775\ cm^{-1}$ and $\gamma = 150\ mJ/K^2$ mole [17], while for U_2Zn_{17} $m^* = 36 m_b$ and $n_e = 2 \times 10^{21}\ cm^{-3}$ using $\omega_p^* = 2178\ cm^{-1}$ and $\gamma = 395\ mJ/K^2$ mole [12]. For UPd_2Al_3, our estimate of m* is in fair agreement with the evaluation in [17] by combining specific heat with upper critical field investigations, and in [42] with de Haas van Alphen measurements. Particularly, the value of n_e corresponds, in the case of $m_b = m_e$, to a high temperature (i.e., at $T \gg T_{CO}$) plasma frequency of $\omega_p = 4.76 \times 10^4\ cm^{-1}$ (5.9 eV). Indeed, at 300 K and also at 20 K we have fitted our optical conductivity, decoupled from the huge mid-IR absorption at $2000\ cm^{-1}$ with $\omega_p = 4.4 \times 10^4$ (5.4 eV) cm^{-1} (Table 1)

We can now apply sum rule or spectral weight arguments and compare the plasma frequency at 300 K with the renormalized ω_p^* at temperatures lower than T_N. This leads to the expression:

$$\left(\frac{\omega_p(300\ K)}{\omega_p^*}\right) = \sqrt{\frac{m^*}{m_b}}\sqrt{\frac{n(300\ K)}{n(T < T_N)}} \qquad (7)$$

With the assumption that the total charge carrier concentration does not change below T_{CO} and above all below T_N, i.e. $n(300\ K) = n(T < T_N)$, because the Fermi surface is unaffected by the AFM transition (see below), we obtain $m^*/m_b \sim 85$ and 41 at 6 K for UPd_2Al_3 and for U_2Zn_{17}, respectively, in good agreement with previous evaluations [11, 17, 42]. Consequently, UPd_2Al_3 and U_2Zn_{17} can be considered as moderate heavy electron systems. Similar optical results have recently been obtained for the compound UNi_2Al_3 [43]. In the low-temperature coherent region, a narrow Drude-like, quasiparticle absorption mode develops and an enhancement of the effective mass of about 50 was inferred [43].

Since the temperature dependence of $\sigma_1(\omega)$ is not affected by the onset of the AFM transition, we tend to ascribe U_2Zn_{17} and UPd_2Al_3 to the class of materials with an AFM order among localized moments. In other words, the behaviour of $\sigma_1(\omega)$ in the latter two compounds is indicative of the fact that the AFM transition is *not* the consequence of the $2k_F$ nesting of the Fermi surface (or part of it) and thus is not a Fermi surface instability which could lead to an itinerant antiferromagnetic ground state, like a SDW condensate. This latter scenario would imply the partial opening of a gap of the order of $2\Delta \sim 3.5 k_B T_N$ on the Fermi surface. The dc resistivity also indicates the absence of a Fermi surface anomaly, and reflects the freezing out of the spin-flip scattering mechanism and the increase of the relaxation time τ [44]. In this respect, it is interesting to note that UNi_2Al_3, which can be considered as a sister compound of UPd_2Al_3, does show a weak anomaly in $\rho(T)$ at T_N [35], instead of the simple change of slope for UPd_2Al_3. A μSR investigation of UNi_2Al_3 seems to support the formation of a SDW condensate at T_N [41], indicating therefore an AFM phase transition of itinerant nature. So far the optical investigations were performed above T_N [43], and it would be of interest to compare the excitation spectrum of UNi_2Al_3 below T_N with that of UPd_2Al_3.

Unless an eventual SDW-like gap absorption develops at very and thus anomalously low frequencies (i.e., outside the measured frequency spectral range), we anticipate that the situation in UPd_2Al_3 and U_2Zn_{17} is very different to what occurs in UCu_5 and URu_2Si_2 (see below). The existence of a low frequency SDW-like gap absorption seems also to be ruled out by any other experimental data. Nevertheless, it cannot a priori be excluded that this localized antiferromagnetic order still opens high frequency gaps in the electronic band structure, due to the crystal potential and depending on the degree of interaction between possible new boundaries of the Brillouin zone (BZ) and the Fermi surface (i.e., depending on whether the zone boundaries only touch or cut the Fermi surface) [45]. However, this possibility is very unlikely at least for U_2Zn_{17} since its magnetic BZ has been claimed to be identical with the chemical zone [46].

b) $UCu_{5-x}Ni_x$ and $URu_{2-x}Re_xSi_2$

The striking feature in $\sigma_1(\omega)$ of UCu_5 and URu_2Si_2 is the appearance of a new absorption in the FIR by lowering the temperature below T_N, in contrast to the experimental findings discussed above for the U_2Zn_{17} and UPd_2Al_3 compounds. In addition a narrow Drude-like resonance develops from the FIR spectral range down to zero frequency. Using the phenomenological Lorentz-Drude approach of (5), we ascribe a Drude term to the low frequency narrow resonance and a minimum set of h.o. to the various absorptions at higher frequencies. We tend to ascribe those to electronic interband transitions, even though a complete band structure calculation would be of help for a precise identification of these absorptions. By lowering the temperature below T_N one has to introduce an additional h.o. in order to fully describe $\sigma_1(\omega)$. The relevant fit parameters, i.e., for the Drude term and the resonance frequency 2Δ of the absorption appearing below T_N, are summarized in Table 1 for both compounds.

Figure 10 displays $\sigma_1(\omega)$ of UCu_5 at various temperatures in the FIR together with the phenomenological fits. At 6 and 9 K we also plot separately the two relevant components of the fit: the low frequency Drude term and the h.o. for the new absorption appearing below T_N. At 6 K, the asymmetric shape of the FIR absorption cannot be completely reproduced by the Lorentz h.o. Nevertheless, this simple phenomenological approach can reproduce the relevant trends of the data and clearly points out the necessity to include the additional absorption below T_N (see Fig. 10c–e). It must be stressed that the FIR

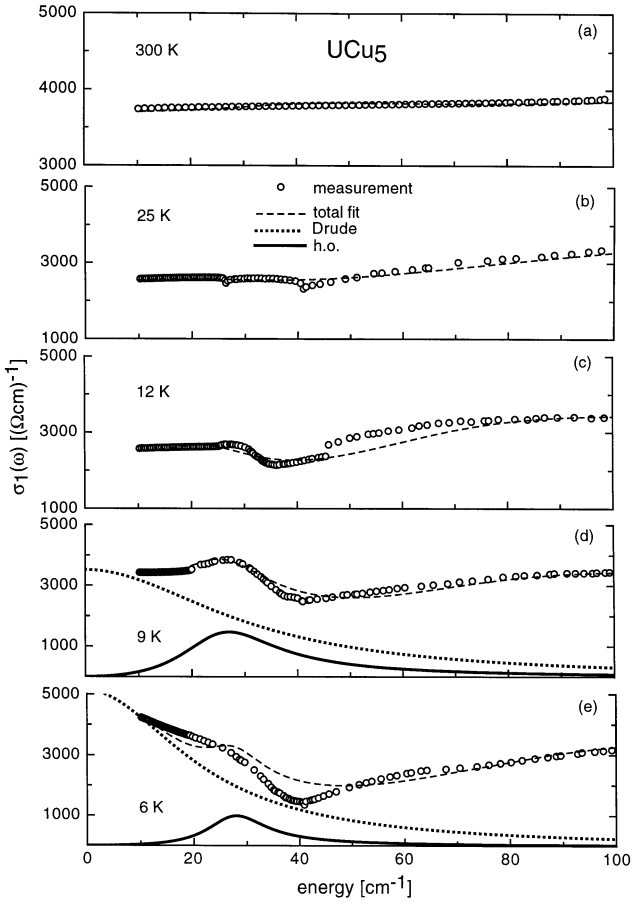

Fig. 10a–e. Optical conductivity at several temperatures in the FIR energy range (linear energy scale) for UCu_5, together with the phenomenological fits. At 6 and 9 K, we display the Drude and h.o. components separately (see text and Table 1 for the fit parameters). The small discontinuities at 27 and 41 cm^{-1} at 25 K, and at 45 cm^{-1} at 12 K are due to the scattering in the original reflectivity data

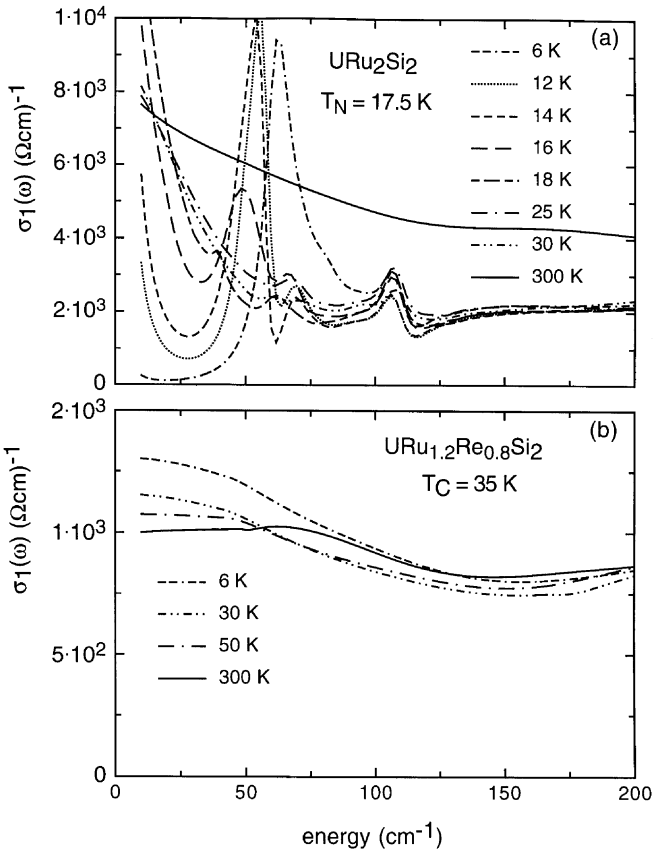

Fig. 11. Optical conductivity in FIR of $URu_{2-x}Re_xSi_2$ for **a** x = 0 and **b** x = 0.8 at various temperatures

absorption below T_N for UCu_5 is not due to a so-called "plasma-edge" effect. One might argue that strong phonon modes or electronic interband transitions in UCu_5 might shift the plasma frequency to such a low spectral range, inducing a broad hump in the reflectivity spectra. In other words, if the screening of the plasma frequency by phonon absorption and/or electronic interband transitions is strong enough, the so-called zero crossing of $\varepsilon_1(\omega)$ with $d\varepsilon_1(\omega)/d\omega > 0$ will be shifted down to the FIR, consequently making possible the formation of a plasma edge behaviour at such low frequencies. We have checked this issue within our phenomenological approach (5). A consistent fit of the data cannot be reached without the addition of the FIR absorption which appears below T_N. This rules out the possibility that high-frequency interband transition or phonon modes alone can account for the sudden enhancement of the reflectivity below about 50 cm^{-1}. A similar situation is found in URu_2Si_2 (Figs. 6 and 11a). However, the two components (i.e., the Drude term at low frequencies and the FIR absorption appearing below T_N) in $\sigma_1(\omega)$ are well separated and more distinct than in UCu_5 for which the FIR absorption is most clearly seen at 9 K.

We claim therefore, that the temperature dependence of $\sigma_1(\omega)$ in the FIR of UCu_5 and URu_2Si_2 is related to the onset of the AFM order below T_N. The FIR excitation is interpreted as being due to a SDW gap [28, 29], implying the partly itinerant nature of the AFM phase transition at T_N. As far as URu_2Si_2 is concerned, the SDW gap at 60 cm^{-1} was also clearly identified with point contact spectroscopy (PCS) measurements. These experimental findings are suggestive of a BCS-like SDW gap in the density of states (DOS) below T_N [32, 47, 48]. This interpretation is analogous to what has been suggested for Cr [25]. There is also a compelling similarity with the optical properties of UNi_2Si_2 [49]. UNi_2Si_2 has a complex magnetic phase diagram. Particularly, at 124 K an incommensurate AFM order develops and optical measurements clearly indicate the opening of a gap at 280 cm^{-1} in FIR [49], which has been also associated with a SDW-like gap excitation.

Based on the phenomenological fit of (5), we evaluate the resonance frequency, ascribed to excitations across the SDW gap. Its saturation value for UCu_5 is 28 cm^{-1} and for URu_2Si_2 it is 63 cm^{-1} corresponding to renormalized gaps of $2\Delta/k_BT_N = 2.7$ and 5.3 for UCu_5 and URu_2Si_2, respectively. The gap ratio for UCu_5 is in agreement with a previous evaluation arrived at by an analysis of $\rho(T)$ around T_N, assuming a two-component description of the total conductivity [23]. This latter analysis also suggests that only 20% of the total charge-carrier concentration

above T_N is involved in the SDW phase transition. Hence, the remaining free charge carriers (i.e., $\sim 80\%$) contribute to the optical conductivity with the low frequency Drude behaviour. This contribution overlaps the SDW gap absorption. Indeed at 6 K, the SDW-gap in UCu_5 appears at best as a shoulder. At 6 K, σ_{dc} is two times larger than it is at T_N and the Drude contribution partially smears the SDW gap absorption. The decaying magnetic scattering and the onset of coherence, as the heavy-electron state develops well below T_N, enhance the scattering relaxation time, making the Drude component narrower and narrower. With the development of the many-body correlated state one actually associates the low frequency narrow Drude-like resonance with the so-called "renormalized" Drude contribution (see our previous discussion for UPd_2Al_3 and U_2Zn_{17}). From the plasma frequency at 300 K and the renormalized one at 6 K (Table 1), we can also evaluate the enhancement of the effective mass of the "heavy" quasiparticles in UCu_5. By applying eq. (7) with $n(T < T_N)/n(300\ K) \sim 0.8$, we found $m^* = 95\ m_b$ at 6 K indicating that UCu_5 is a moderate heavy-electron system.

In analogy to UCu_5, the effective mass enhancement of the heavy quasiparticles in URu_2Si_2 at low temperature can be evaluated by assuming that 70% of the total charge carrier concentration survives the formation of the SDW condensate (i.e., $n(T < T_N)/n(300K) \sim 0.7$), as suggested by the dc transport measurement [15]. From (7), we found a value $m^* = 68m_b$ which is consistent with the dc-limit of $m^*(\omega)$ of a previous analysis [28], performed by applying a so-called generalized Drude approach (i.e., where τ and m^* are allowed to be frequency dependent). An equivalent evaluation of m^* for both URu_2Si_2 and UCu_5 can be also achieved by comparing the normalized plasma frequency ω_p^* with the specific heat γ values [12, 15, 23].

As already pointed out, the SDW-gap absorption in URu_2Si_2 is more distinct from the normalized Drude resonance than in UCu_5. This is ascribed to the fact that in URu_2Si_2 the many-body correlated state and its heavy quasiparticles have already developed (i.e., $T_N < T_{CO}$) while in UCu_5 the onset of the correlated-state regime virtually coincides with the AFM phase transition (i.e., $T_N = T_{CO}$). Nevertheless, in both compounds the total spectral weight in $\sigma_1(\omega)$ is conserved. This means that below T_N there is a shift of spectral weight from the Drude component towards the FIR absorption. Anyway, the well resolved SDW-gap absorption from the remaining free charge carriers contribution in URu_2Si_2 allows us to extract quite precisely the temperature dependence of the gap excitation for the itinerant antiferromagnetic phase. It is clear from Fig. 11a that the low-temperature FIR absorption shifts to lower frequencies and broadens for increasing temperature towards T_N. The temperature dependence of the resonance frequency ($\omega_1 = 2\Delta$) of the FIR absorption in $\sigma_1(\omega)$, determined by applying (5), is shown in Fig. 12, where we also compare the experimental temperature dependence of Δ with the BCS theory [50]. There is reasonable agreement, even though our evaluation of $\Delta(T)$ deviates from the theoretical prediction for T close to T_N. Experimentally, this is a quite common situation, which can be ascribed to various effects. The important role played by thermal smearing and inhomogeneous distribution of T_N in the samples

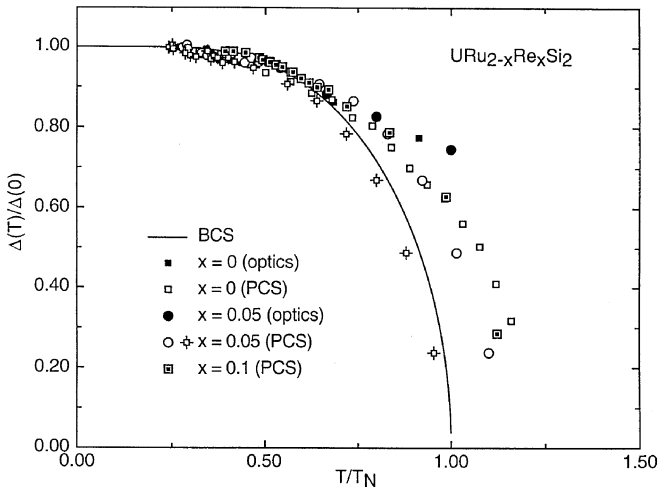

Fig. 12. Temperature dependence of the SDW-gap for $URu_{2-x}Re_xSi_2$ ($x < 0.2$), evaluated from the optical and PCS spectra [32] and compared with the BCS theory. We have used $T_N = 17.5$ K, 15 K and 10.5 K for x = 0, 0.05 and 0.1, respectively [27]. For x = 0.05, we also show the $\Delta(T)/\Delta(0)$ ratio evaluated from the PCS spectra, assuming $T_N = 17.3$ K (⊹) instead of 15 K (○)

lead immediately to an enhancement of the gap value with respect to the BCS expectation when T_N is approached from below [32]. For T_N's slightly larger than the reported values, the agreement of $\Delta(T)/\Delta(0)$ with the BCS theory would be outstanding. It was also shown that the temperature dependence of Δ inferred from the optical data coincide with $\Delta(T)$ evaluated from the temperature dependence of the point contact spectra [32].

A further confirmation of the SDW-gap scenario comes from our experiments in the doped materials, i.e. UNi_xCu_{5-x} and $URu_{2-x}Re_xSi_2$. The FIR absorption disappears upon doping (Figs. 5, 7, 11b). Here, we particularly focus our attention on the ferromagnetic phase for $URu_{2-x}Re_xSi_2$ ($x > 0.4$). Figure 11b shows the representative example of x = 0.8 which is characterized by a Curie temperature of $T_C = 35$ K. The ferromagnetic state corresponds to a $q = 0$ phase transition, and, therefore, contrary to the itinerant antiferromagnetic phase transition due to a $q = 2k_F$ anomaly, the Fermi surface is not involved. Consequently, the opening of a gap at the Fermi level ε_F is not expected. The suppression of the spin-flip scattering mechanism in coincidence with the onset of the ferromagnetic order leads at most to an enhancement of the scattering relaxation time (i.e., a narrowing of the Drude-like resonance in $\sigma_1(\omega)$ at low frequencies), similar to the situation met for the antiferromagnetic ordering of localized type (see the discussion for UPd_2Al_3 and U_2Zn_{17}, Figs. 8 and 9). Our recent point contact-spectroscopy) investigation further supports this interpretation, since the BCS-like gap in DOS of URu_2Si_2 disappears upon Re-doping [32].

Finally, we briefly comment on the shape of the SDW gap excitation, seen in $\sigma_1(\omega)$, which is rather sharp (Fig. 11a). This is very distinct from what would be expected for a simple three dimensional semiconductor [39]. Besides dimensionality effects, the sharp gap excitation might be the consequence of the so-called coherence factor

effects encountered in the BCS formalism [50, 51]. In fact, spin- and charge-density-wave condensates can be described within the same meanfield BCS-like formalism, as conventional superconductors [51]. The coherence factors associated to the electromagnetic response are, however, different for a superconductor (case II) than for a CDW or SDW condensate (case I). Such a difference arises because for a SDW (or alternatively a CDW) condensate the nesting of the Fermi surface lead to an electron-hole pairing with total $q = 2k_F$, while in a superconductor the Cooper pair corresponds to a two electron object with $q = 0$ [50, 51]. The difference in the coherence factors is also reflected in the shape of $\sigma_1(\omega)$, which has a smooth onset of absorption at the gap for a superconductor (i.e., very much similar to a three dimensional semiconductor) and a sharp feature for a CDW and SDW condensate. It is rather compelling to note that there is a striking similarity between the magnetic gap feature of URu_2Si_2 and of the prototype one-dimensional SDW systems, like the organic $(TMTSF)_2PF_6$ compound [51, 52]. The optical response of this latter compound is well described by a BCS-type calculation assuming a case I coherence factor [50, 52]. Correlation effects due to the mixing between the f states and the extended bands, and also crystallographic anisotropy might eventually enhance the sharp peak feature of the SDW-gap absorption. However, it remains to be seen to which extent optics can alone distinguish between these different possibilities.

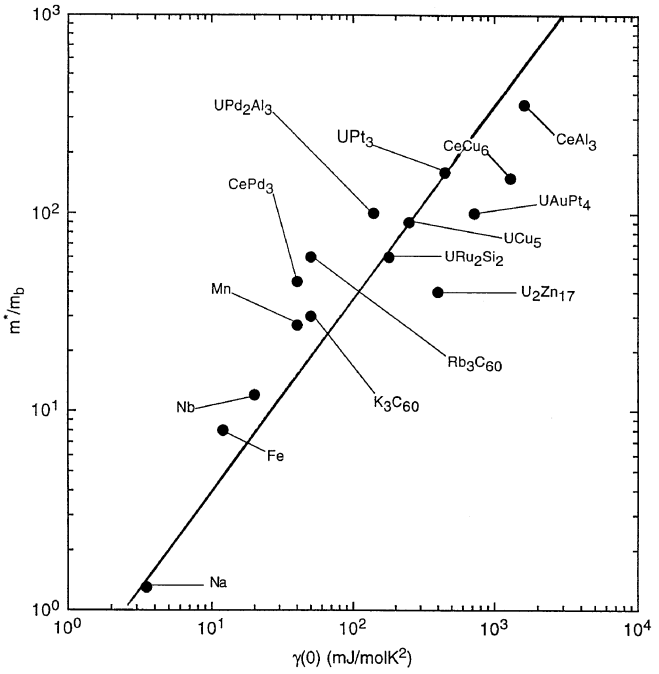

Fig. 13. Specific heat γ values [11–14, 17, 23, 26, 53] versus effective mass m* evaluated from the optical data using spectral weight arguments (see text)

Conclusions

We have measured the complete electrodynamic response of a series of heavy-electron antiferromagnets at temperatures below T_{CO}, and in the temperature regime where the AFM phase transition takes place. First of all, in the correlated state (i.e., below T_{CO}), $\sigma_1(\omega)$ for all compounds displays the typical feature expected for the excitation spectrum of heavy quasiparticles. In fact, by lowering the temperature below T_{CO}, there is a progressive appearance of a narrow Drude-like resonance. This resonance is fully developed at temperatures lower than T_{CO}. The renormalized Drude-like nature of the resonance indicates excitations of the heavyquasiparticles as its origin. We have extracted several intrinsic parameters (m* and τ*) characterising this coherent many-body state, and find that the enhancement of the effective mass of the heavy quasiparticles is in full agreement with corresponding thermodynamic results. Figure 13 shows the specific heat $\gamma(T \rightarrow 0)$ values [11–14, 17, 23, 26, 53] versus the effective mass m* of the heavy quasiparticles extracted from the optical data with the spectral weight analysis. The γ vs m* representation is alternative to γ vs the $T = 0$ magnetic suspectibility $\chi(0)$ or vs the coefficient A of the T^2-behaviour in the resistivity $\rho(T)$, which are mostly used. Our choice (Fig. 13) allows us to compare magnetic with non-magnetic system in the same framework. It clearly appears that also the moderate heavy-electron materials undergoing magnetic ordering have γ values nearly scaling with m*. The deviations from $\gamma \sim$ m* (which are not systematic) might be explained by the fact that we compare the outcome of different experimental techniques applied to specimens of different origin. However, the fact that the heavy-electron antiferromagnet materials fall on the same line with other more conventional or prototype heavy-electron compounds indicates a kind of universal behaviour. In fact, the "free-electron" relation between γ and m* holds and, in our particular case, does not seem to be affected by the onset of magnetic ordering.

As far as the AFM phase transition is concerned, we have shown that the electrodynamic response is indicative of the different nature of the AFM phase transitions, observed in these compounds. There is an interesting analogy between the excitation spectra of UCu_5 and URu_2Si_2, and between that of U_2Zn_{17} and UPd_2Al_3, which obviously is also reflected in the corresponding different behaviours of $\rho(T)$. Our experiments on UPd_2Al_3 and U_2Zn_{17} do not give evidence for a SDW energy gap. This is in accordance with the antiferromagnetic order of localized type [16, 17, 53], implying that in UPd_2Al_3 and U_2Zn_{17} the magnetic ground state develops by interactions other than electron-electron interactions related to the Fermi surface [11]. Transport and specific heat measurement [53] and a recent photoemission investigation on UPd_2Al_3 [54] suggest the coexistence of two subsystems with more localized 5f states responsible for the magnetic properties and less localized states responsible for the formation of heavy electrons and then for the superconducting properties. UPd_2Al_3 and U_2Zn_{17} are fundamentally different from UCu_5 and URu_2Si_2, where the opening of a SDW-like gap and the increase of $\rho(T)$ just below T_N is indicative of an antiferromagnetic order invoking itinerant quasiparticles [29].

Nevertheless, it remains to be seen what kind of relation may be established between typical itinerant features

in the electrodynamic response of these antiferromagnets, particularly of UCu_5 and URu_2Si_2, and their rather simple magnetic order, apparently commensurate with the lattice [18–21]. One possible way to reconcile the optical results with the neutron scattering is to consider for simplicity a one dimensional model [51]. For a strictly half filled band, Coulomb correlations lead to an insulating, and commensurate magnetic ground state. In this case, the Hubbard model is appropriate. Away from half filling, two situations may occur. First of all, an incommensurate SDW state, which would open up a gap at the Fermi level, leading to an insulator, and to an incommensurate magnetic structure, and second, a commensurate SDW state with discommensurations. Broadly speaking, this latter state would have a remaining gap structure, a low energy, translationally invariant excitation and a commensurate magnetic structure. Such a situation bears some similarities with that of a doped insulator.

We believe that the HE antiferromagnets may be similar to the second situation, sketched above. Here, the gap is associated with the commensurate regions and can be seen if it falls into the region of the Fermi energy. This may be the appropriate description for URu_2Si_2 and UCu_5. When the Fermi level does not lie inside the gap, the excitation across the gap cannot be seen by optical experiments, and this may be the situation for UPd_2Al_3 and U_2Zn_{17}. This scenario is also close to what is expected for a single, partially filled band where the period doubling due to the magnetic structure leads to a gap away from the Fermi level [44].

A host of interesting questions remains to be solved. One aspect to inquire further is the nature of the translationally invariant excitations. In a strictly one-dimensional model these are soliton type excitations [51] but in higher dimensions they may eventually have single particle character. Moreover, the details of the magnetic, commensurate ground state needs more precise investigations. Different experiments (e.g., neutron scattering and μSR) can reveal novel magnetic features and rather complex magnetic ordering. Particular emphasis should be devoted to the possible effect of the translationally invariant excitations on the magnetic structure. Finally, besides the issues raised above, the interplay between single particle character and many body correlation effects are of relevant importance for a full understanding of the magnetic state of heavy-electron magnets. In this respect, it remains to be seen how important is the role of exchange interactions, like, e.g., in the so-called three-spin correlator model, suggested by Gor'kov [55], in order to explain the weak antiferromagnetism and the small magnetic moments ($\sim 10^{-2}\,\mu_B$) in some heavy-electron systems, like URu_2Si_2.

The authors wish to thank P. Wachter for important financial support, T.M. Rice, R. Hlubina and R. Monnier for helpful discussions, and J. Müller for technical assistance. The work is also part of a joint collaboration under the auspices of a grant by the Swiss-U.S. National Foundations for the Scientific Research. The research at UCSD was supported by the U.S. Department of Energy under Grant No. DE-FG03-86ER-45230 and the National Science Foundation under Grant No. DMR-9209668.

References

1. Webb, B.C., Sievers, A.J., Mihalisin, T.: Phys. Rev. Lett. **57**, 1951 (1986)
2. Marabelli, F., Travaglini, G., Wachter, P.: Solid State Commun. **59**, 381 (1986)
3. Sulewski, P.E. Sievers, A.J., Maple, M.B., Torikachvili, M.S., Smith, J.L., Fisk, Z.: Phys. Rev. B**38**, 5338 (1988)
4. Marabelli, F., Wachter, P., Walker, E.: Solid State Commun. **67**, 931 (1988)
5. Awasthi, A.W., Beyerman, W., Carini, J.P., Gruner, G.: Phys. Rev. B**39**, 2377 (1989)
6. Marabelli, F., Wachter, P.: Phys. Rev. B**42**, 3307 (1990)
7. Marabelli, F., Wachter, P.: Physica B**163**, 224 (1990)
8. Awasthi, A.M., Degiorgi, L., Güner, G., Dalichaouch, Y., Maple, M.B.: Phys. Rev. B**48**, 10692 (1993)
9. Lee, P.A., Millis, A.J.: Phys. Rev. B**35**, 3394 (1987)
10. Fukuyama, H.: in: Theory of heavy fermions and valence band fluctuations, p. 209. Kasuya, T., Saso, T. (eds.). Berlin, Heidelberg, New York: Springer 1985
11. Ott, H.R., Rudigier, H., Delsing, P., Fisk, Z.: Phys. Rev. Lett. **52**, 1551 (1984)
12. Ott, H.R., Rudigier, H., Felder, E., Fisk, Z., Batlogg, B.: Phys. Rev. Lett. **55**, 1595 (1985)
13. Grewe, N., Steglich, F.: in: Handbook on the Physics and Chemistry of rare earths, Vol. 14. Gschneider, K.A., Eyring, L., (eds.). Amsterdam: Elsevier 1991
14. Fisk, Z., Hess, D.W., Pethick, C.J., Pines, D., Smith, J.L., Thompson, J.D., Willis, J.O.: Science **239**, 33 (1988); Ott, H.R.: J. Mod. Phys. B**6**, 473 (1992)
15. Maple, M.B., Chen, J.W., Dalichaouch, Y., Kohara, T., Rossel, C., Torikachvili, M.S.: Phys. Rev. Lett. **56**, 185 (1986)
16. Geibel, C., Thies, S., Kaczorowski, D., Mehner, A., Grauel, A., Seidel, B., Ahlheim, U., Helfrich, R., Petersen, K., Bredl, C.D., Steglich, F.: Z. Phys. **83**, 305 (1991)
17. Geibel, C., Schank, C., Thies, S., Kitazawa, H., Bredl, C.D., Boehm, A., Rau, M., Grauel, A., Caspary, R., Helfrich, R., Ahlheim, U., Weber, G., Steglich, F.: Z. Phys. B **84**, 1 (1991)
18. Murasik, A., Ligenza S., Zygmunt, A.: Phys. Status Solidi a**23**, K163 (1974)
19. Schenck, A., Birrer, P., Gygax, F.N., Hilti, B., Lippelt, E., Weber, M., Boeni, P., Fischer, P., Ott, H.R. Fisk, Z.: Phys. Rev. Lett. **65**, 2454 (1990)
20. Kjems, J.K., Broholm, C.: J. Magn. Magn. Mater. **76–77**, 371 (1988)
21. Krimmell, A., Loidl, A., Roessli, B., Doenni, A., Kita, H., Sato, N., Endoh, Y., Komatsubara, T., Geibel, C., Steglich, F.: Solid State Commun. **87**, 829 (1993)
22. Schenck, A., Amato, A., Birrer, P., Gygax, F.N., Hitti, B., Lippelt, E., Barth, S., Ott, H.R., Fisk, Z.: J. Magn. Magn. Mater. **108**, 97 (1992)
23. Bernsconi, A., Mombelli, M., Fisk, Z., Ott, H.R.: Z. Phys. B**94**, 423 (1994)
24. Palstra, T.T.M., Menovsky, A.A., Mydosh, J.A.: Phys. Rev. B**33**, 6527 (1986)
25. Barker Jr. A.S., Halperin, B.I., Rice, T.M.: Phys. Rev. Lett. **20**, 384 (1968)
26. Ott, H.R., Fisk, Z.: Handbook on the physics and chemistry of the actinides p. 85. (Eds.) A.J. Freeman and G.H. Lauder Elsevier Science Publishers B.V. (1987)
27. Dalichaouch, Y., Maple, M.B., Torikachvili, M.S., Giorgi, A.L.: Phys. Rev. B**39**, 2433 (1989)
28. Bonn, D.A., Garrett, J.D., Timusk, T.: Phys. Rev. Lett. **61**, 1305 (1988)
29. Overhauser, A.W.: Phys. Rev. **128**, 1437 (1962)
30. Degiorgi, L., Dressel, M., Grüner, G., Wachter, P., Sato, N., Komatsubara, T.: Europhys. Lett. **25**, 311 (1994)
31. Degiorgi, L., Ott, H.R., Dressel, M., Gruner, G., Fisk, Z.: Europhys. Lett. **26**, 221 (1994)
32. Thieme, St., Steiner, P., Degiorgi, L., Wachter, P., Dailchaouch, Y., Maple, M.B.: Europhys. Lett. **32**, 367 (1995) and Europhys. lett. **32**, 783 (1995) (Erratum)

33. Klein, O., Donovan, S., Dressel, M., Gruner, G.: Int. J. Infrared Millimeter Waves **14**, 2423 (1993); Donovan, S., Klein, O., Dressel, M., Holczer, K., Gruner, G.: ibid **14**, 2459 (1993); Dressel, M., Klein, O., Donovan, S., Gruner, G.: ibid **14**, 2489 (1993)
34. Degiorgi, L., Ott, H.R., Dressel, M., Grüner, G., Geibel, C., Steglich, F., Fisk, Z.: Physica B**206**–**207**, 441 (1995)
35. Dalichaouch, Y., de Andrade, M.C., Maple, M.B.: Phys. Rev. B**46**, 8671 (1992)
36. Awasthi, A.M., Beyermann, W.P., Carini, J.P., Gruner, G.: Phys. Rev. B**39**, 2377 (1989)
37. Sulewski, P.E., Sievers, A.J.: Phys. Rev. Lett. **63**, 2000 (1989)
38. Beyermann, W.P., Gruner, G.: Phys. Rev. Lett. **63**, 2001 (1989)
39. Wooten, F.: Optical properties of solids. New York: Academic Press 1972
40. Sandratskii, L.M., Kübler, J., Zahn, P., Mertig, I.: Phys. Rev. B**50**, 15834 (1994)
41. Uemura, Y.J., Luke, G.M.: Physica B**186**–**188**, 223 (1993)
42. Inada, Y., Ishiguro, A., Kimura, J., Sato, N., Sawada, A., Komatsubara, T., Yamagami, H.: Physica B**206**–**207**, 33 (1995)
43. Cao, N., Garrett, J.D., Timusk, T., Liu, H.L., Tanner, D.B.: Phys. Rev. B**53**, 2601 (1996)
44. The reader should note that the SDW single particle gap (which is missing in $\sigma_1(\omega)$ of UPd_2Al_3 and U_2Zn_{17}) should not be confused with the gap of about 80 K (or 40 K in [35]) evaluated from the analysis of the $\rho(T)$ measurement below T_N. The latter corresponds to the gap in the magnon dispersion relation and has nothing to do with the gap which should open at the Fermi surface as consequence of a SDW instability. See, e.g., Ref. 35 and Bakker, K., de Visser, A., Tai, L.T., Menovsky, A.A., Franse, J.J.M.: Solid State Commun. **86**, 497 (1993)
45. Elliott, R.J., Wedgwood, F.A.: Proc. Phys. Soc. **81**, 846 (1963)
46. Cox, D.E., Shirane, G., Shapiro, S.M., Aeppli, G., Fisk, Z., Smith, J.L., Kjems, J., Ott, H.R.: Phys. Rev. B**33**, 3614 (1986)
47. Hasselbach, K., Kirtley, J.R., Lejay, P.: Physica B**186**–**188**, 201 (1993)
48. Nowack, A., Naidyuk, Yu.G., Chubov, P.N., Yanson, I.K., Menkovsky, A.: Z. Phys. B**88**, 295 (1992)
49. Cao, N., Garrett, J.D., Timusk, T.: Physica B**191**, 263 (1993)
50. Tinkham, M.: Introduction to superconductivity. Krieger, R.E. (ed.). New York: McGraw-Hill 1975
51. Gruner, G.: Density waves in solids. Reading, Mass: Addison-Wesley 1994
52. Degiorgi, L., Dressel, M., Schwartz, A., Alavi, B., Gruner, G.: Phys. Rev. Lett. **76**, 3838 (1996)
53. Caspary, R., Hellmann, P., Keller, M., Sparn, G., Wassilew, C., Koehler, R., Geibel, C., Schank, C., Steglich, F., Phillips, N.E.: Phys. Rev. Lett. **71**, 2146 (1993)
54. Takahashi, T., Sato, N., Yokoya, T., Chainani, A., Morimoto, T., Komatsubara, T.: J. Phys. Soc. Jpn. **65**, 156 (1996)
55. Gor'kov, L.P.: Europhys. Lett. **16**, 301 (1991)